Journal of ELECTRONIC MATERIALS, Vol. 47, No. 1, 2018
DOI: 10.1007/s11664-017-5762-8

Physical Properties of Superhard Diamond-Like BC_5 from a First-Principles Study

IREM O. ALP[1] and YASEMIN O. CIFTCI[1,2]

1.—Department of Physics, Gazi University, Teknikokullar, 06500 Ankara, Turkey. 2.—e-mail: yasemin@gazi.edu.tr

The first-principles calculations are carried out to investigate the structural, elastic, electronic, optical, vibrational and thermodynamic properties of superhard diamond-like BC_5 (d-BC_5). The structural stability of BC_5 is examined for previously proposed and several probable phases including F-43m, P6/mmm, Cmcm, Pnma, P-1, P3m1, Imm2, I-4m2 and Pmma. The most energetically stable phase is predicted to be Pmma. Computed bulk modulus B, shear modulus G, elastic constant C_{44} and theoretical Vickers hardness H confirm that BC_5 is an ultra-incompressible and superhard material. The electronic character analysis reveals the metallicity of BC_5, indicating that a strong covalent bond network through sp^3 hybridization is the origin of its excellent mechanical properties. However, P-1 is found to be dynamically stable, contrary to the other study. Therefore, the phonon, thermodynamic and electronic properties of P-1 which are not available in the literature are discussed. The calculated physical parameters are in good agreement with the theoretical and experimental results. This work is expected to provide a useful guide for designing novel boride materials having superior mechanical performance.

Key words: Superhard boron/carbon materials, elastic properties, electronic properties, vibrational properties

INTRODUCTION

Diamond has been attractive for scientific research and a large variety of applications in industry[1–6] due to its extraordinary physical properties, besides being the hardest known material and exhibiting superconductivity via heavy boron doping.[7,8] However, its chemical characteristics cause two significant problems: poor oxidation resistance and a tendency to interact with ferrous metals.[9] Therefore, diamond-like compounds have aroused considerable interest in the research on prediction and synthesis of new superhard candidates in recent years.[10–14] These more thermally and chemically stable structures obtained by high-temperature and high-pressure technology carry great potential in machining processes, such as cutting, shaping, hard coating and abrasive blasting.[15–19] Furthermore, nowadays porous materials based on boron, carbon and nitrogen (B, C and N) have become the center of attention as a result of their usage in rechargeable metal-air batteries and fuel cells for renewable energy production, as well as biomedical sciences and electronics.[20–23]

Due to being a member of the family mentioned above, there have been numerous theoretical articles related to BC_5. The available research data is based mostly on one set of experimental evidence[24] with the aim of clearing up the crystal structure of the material. In consequence of the continual efforts on seeking low-energy crystals, Solozhenko et al. synthesized a superhard cubic BC_5 (c-BC_5) phase with a lattice parameter a = 3.635 Å, a high bulk modulus of 335 GPa and a Vickers hardness of 71 GPa.[24] Accordingly, in theory, the considered diamond-like BC_5 compound (d-BC_5) is formed by substituting a B atom for one of the C atoms

(Received January 27, 2017; accepted August 22, 2017; published online September 7, 2017)

tetrahedrally (sp^3) bonded to four neighbors in a six-atom supercell. This hexagonal lattice contains three rhombohedron diamond primitive unit cells, and the parameters resulted from the optimization process match up with that of c-BC_5.

Even so, there is still some complexity owing to missing important details, such as space groups, atomic coordinates, etc. in most of the papers. At this point, it has been necessary to give information about the theoretical explorations in order to clarify the structural classification and evaluate all findings together: (1) The structural and electronic properties of hexagonal[25–27] and orthorhombic[28] BC_5 with possible configurations have been presented. (2) The superconducting character of P3m1,[29] I-4m2[31] and two constructions for Pmma[36] has been proposed with an estimated 45 K, 47 K, ~11 K and ~23 K of critical temperature, respectively. (3) The mechanical stability,[30,32,33,37,38] and electronic behavior[32,38] of ultra-incompressible superhard P3m1 have been studied. (4) The high-pressure effect on the physical properties, stability[39,41] and optical parameters[40] of P3m1 and I-4m2 have been examined.

Meanwhile, Xi et al. put forward that Pmma is more stable than I-4m2, predicted to be the most stable one theoretically at that time,[35] and Mikhaylushkin et al.[42] have suggested a structural model of BC_5 via global space-group optimization method with lower energy than that claimed by Li et al.[36] Most recently, Li et al. reported structural and electronic properties of Pmma in the discussion about superhard B_xC_y compounds.[43]

In this letter, the first-principles study within well-converged *ab initio* calculations on the ground-state properties has been investigated comprehensively with the purpose of revealing the physical characterization of BC_5. The optimized unit cells obtained from computation are shown in Fig. 1 and it is found that simple orthorhombic Pmma (space group number: 51) is the most stable one energetically, as Xi et al. have similarly claimed.[35] Moreover, it should be emphasized that the research indicating P-1 phase's being dynamically unstable[31] is in contradiction with the results herein. Thus, electronic, phonon and thermodynamic properties of P-1 along with the elastic properties of Imm2 not considered in related studies[31,36] have been put forth to fill the gap in the literature.

On the other hand, the size of single crystals synthesized so far has not been sufficient because introducing such a large number of boron elements into diamond via the conventional method still seems troublesome from a practical point of view. Hence, theoretical perspective has great importance in determining the BC_5 crystal structure and the characteristics of thermodynamically stable phases.

METHOD OF CALCULATION

All calculations are performed based on the density functional theory utilizing pseudopotential projector augmented wave (PAW)[44,45] method developed by Blöchl[46] to describe the electron–ion interactions within the generalized gradient approximation of Perdew, Burke and Ernzerhof (GGA-PBE)[47] as implemented in the Vienna *ab initio* simulation package (VASP).[48] The wave functions are expanded through a plane-wave basis set with a high cutoff energy of 1000 eV to obtain the greatest accuracy possible. Pseudo-atomic calculations are carried out for B:[He]$2s^2 2p^1$ and C:[He]$2s^2 2p^2$. Numerical integration of the Brillouin zone via the Monkhorst–Pack scheme and k-point meshes[49] are constructed for geometric optimization of the internal coordinates and lattice parameters as well as energy calculations in the ground-state without core correction or spin effect (see Table I). Due to the convergence minimum criterion according to atomic relaxations, it is assumed that the energy difference between two successive iterations is less than 10^{-8} eV per unit cell, and the forces acting on the atoms are less than 10^{-6} eV/Å. Additionally, the mechanical properties are determined from the computed elastic constants with the stress–strain method.[50,51] The phonon properties are calculated using supercell approximations via PHONOPY code.[52]

RESULTS AND DISCUSSION

Structural Properties

As far as is known, the BC_5 compound has been synthesized only in a nanocrystalline form with a cubic system,[24] but authors have come to inconsistent theoretical conclusions, as mentioned in the introduction. Accordingly, we intended to explore new probable phases, the atomic positions of which are assigned by using coordinates corresponding to the suitable Wyckoff positions and site symmetries. The full optimization process is performed with the aim of analyzing the ground-state properties for a great number of candidates besides the ones presented in the literature previously. Then, nine of these phases which have both positive cohesive (E_{coh}) and the lowest total energies are listed in Table I with the space group numbers, crystal systems, k-points and the fractional coordinates used in our study. The k-point meshes are specified by the convergence test that yields the absolute total energy with a precision of less than 10^{-4} eV. Furthermore, one should note that multiplicities of the Wyckoff letters indicate the number of sites per unit cell in this table. The calculated positive E_{coh} values using this equation:

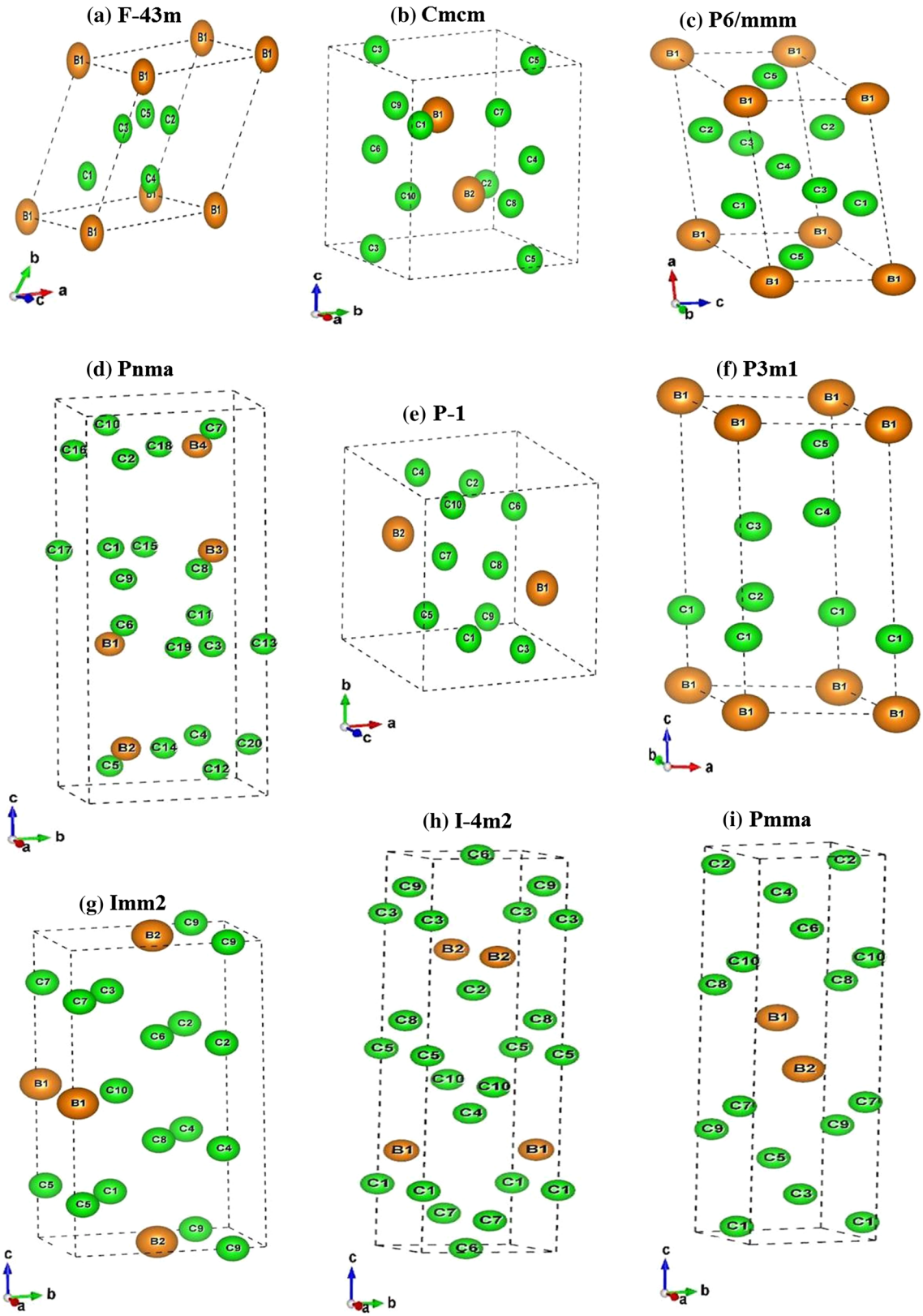

Fig. 1. The primitive unit cells for F-43m (a) and Cmcm (b); the unit cells for P6/mmm (c), Pnma (d), P-1 (e), P3m1 (f), Imm2 (g), I-4m2 (h) and Pmma (i).

Table I. Space group numbers, crystal systems, *k*-points and optimized fractional coordinates (with multiplicities and Wyckoff letters) of nine different phases of BC_5 with references

Phase	Space group no.	Crystal system	*k*-points	Fractional coordinates *x*, *y*, *z*	
F-43m	216	Face centered cubic (fcc)	8 × 8 × 8	0.0000 0.0000 0.0000 B **(4a)**	
				0.2500 0.2500 0.2500 C **(4c)**	
				0.5947 0.5947 0.5947 C **(16e)**	
P6/mmm	191	Hexagonal	9 × 9 × 11	0.0000 0.0000 0.0000 B **(1a)**	
				0.3333 0.6667 0.0000 C **(2c)**	
				0.5000 0.0000 0.5000 C **(3g)**	
Cmcm	63	Base-centered orthorhombic (baco)	6 × 6 × 8	0.0000 0.6964 0.2500 B **(4c)**	
				0.0000 0.9007 0.2500 C **(4c)**	
				0.1894 0.0000 0.0000 C **(8e)**	
				0.7036 0.0836 0.2500 C **(8g)**	
Pnma (Pmcn)	62	Simple orthorhombic (so)	15 × 9 × 4	0.2585 0.2500 0.3737 B **(4c)**	
				0.3124 0.2500 0.6239 C **(4c)**	
				0.2247 0.2500 0.0572 C **(4c)**	
				0.7215 0.2500 0.5622 C **(4c)**	
				0.0241 0.4892 0.6093 C **(8d)**	
P-1	2	Triclinic	13 × 13 × 13	0.1898 0.6055 0.2681 B **(2i)**	31
				0.3149 0.2161 0.8853 C **(2i)**	
				0.6834 0.0967 0.7720 C **(2i)**	
				0.2009 0.2694 0.6015 C **(2i)**	
				0.3170 0.5598 0.5753 C **(2i)**	
				0.1883 0.9363 0.9368 C **(2i)**	
P3m1	156	Hexagonal	15 × 15 × 6	0.0000 0.0000 0.0066 B **(1a)**	29
				0.3333 0.6667 0.3385 C **(1b)**	30
				0.3333 0.6667 0.5819 C **(1b)**	41
				0.6667 0.3333 0.6644 C **(1c)**	
				0.6667 0.3333 0.8998 C **(1c)**	
Imm2	44	Simple orthorhombic (so)	13 × 9 × 4	0.0000 0.0248 0.5000 B **(2b)**	30
				0.0000 0.7834 0.6724 C **(4d)**	
				0.0000 0.0419 0.1685 C **(4d)**	
				0.0000 0.8246 0.0000 C **(2a)**	
I-4m2	119	Simple tetragonal (st)	15 × 15 × 4	0.5000 0.0000 0.2500 B **(2c)**	30
				0.0000 0.0000 0.5000 C **(2b)**	41
				0.0000 0.0000 0.1564 C **(4e)**	
				0.0000 0.0000 0.0802 C **(4e)**	
Pmma	51	Simple orthorhombic (so)	15 × 15 × 4	0.2500 0.5000 0.5583 B **(2f)**	35
				0.2500 0.0000 0.9612 C **(2e)**	
				0.2500 0.5000 0.8827 C **(2f)**	
				0.2500 0.5000 0.1945 C **(2f)**	
				0.2500 0.0000 0.6495 C **(2f)**	
				0.2500 0.0000 0.2746 C **(2f)**	

$$E_{\text{coh}} = E^{\text{B}}_{\text{atom}} + 5E^{\text{C}}_{\text{atom}} - E^{\text{BC}_5}_{\text{total}}, \quad (1)$$

where $E^{\text{B}}_{\text{atom}}$ and $E^{\text{C}}_{\text{atom}}$ are the energies of B and C atoms in freedom states and $E^{\text{BC}_5}_{\text{total}}$ is the total energy of BC_5, denote the possibility of synthesis but also being energetically favorable.

Also, formation energies are defined by the following formula:

$$E_{\text{F}} = E_{\text{BC}_5} - E_{\text{B}} - 5E_{\text{C}}, \quad (2)$$

where E_{BC_5}, E_{B} and E_{C} stand for the total energy of BC_5, the energies per atom in graphite and α-B_{12}, respectively. Even though we expect negative values, the equation gives positive E_{f} for all phases, indicating that they should be metastable having the thermodynamically stable P–T region such as graphite and fullerene[53] in line with the synthesized c-BC_5 at 24 GPa and about 2200 K.[24]

The ground-state bulk properties and cohesive energies are presented in Table II together with the experimental and other theoretical values obtained by different methods. It would be appropriate to note that the angles calculated for the unit cell of P-1 phase in this study are $\alpha = 119.90°$, $\beta = 80.82°$, and $\gamma = 79.78°$, and they are in well agreement with the other reference values as given to be $\alpha = 119.89°$, $\beta = 80.81°$ and $\gamma = 79.80°$.[31] As it is clearly seen in Table II, the obtained equilibrium lattice constants of the lowest energy configurations are in excellent agreement with the available data. After this stage, P3m1 is especially taken into

Table II. Calculated equilibrium lattice constants (a, b, c), bulk modulus (B), the pressure derivative of bulk modulus (B') and cohesive energies (E_{coh}) per one atom with the other theoretical studies for BC_5 phases and experimental values of c-BC_5

Phase	References	a (Å)	b (Å)	c (Å)	B (GPa)	B' (GPa)	E_{coh} (eV/atom)
F-43m	Present	5.8661			127.9	4.20	3.832
P6/mmm	Present	4.5815		2.2965	203.6	4.11	4.352
Cmcm	Present	6.3553	7.6334	4.3874	222.1	3.60	6.579
Pnma	Present	3.0640	4.8144	12.9181	241.6	3.46	6.724
P-1	Present	4.4552	4.4593	4.4607	324.2	3.25	7.452
	VASP-GGA/PBE[31]	4.455	4.459	4.462	370	3.6	
P3m1	Present	2.5523		6.3903	337.2	3.33	7.476
	QEforge-GGA/PBE[29]	2.55		6.375	337	7.24	
	VASP-GGA/PW[30]	2.55		6.39			
	VASP-GGA/PBE[31]	2.553		6.392	379	3.62	
	BSTATE-GGA[32]	2.552		6.392	407	3.58	
	BSTATE-LDA[27]	2.522		6.324	376	3.65	
	VASP-GGA/PBE[33]	2.210			405		
	VASP-GGA[34]	2.161		6.694	388.1		
	VASP-LDA[31]	2.524		6.326	381		
	CASTEP-GGA[35]			6.316	377		
	VASP-GGA/PBE[36]	2.551			407	3.66	
	VASP-GGA/PBE[37]	2.522		6.395	379	3.54	
	VASP-LDA[34]	2.55		6.328	407	3.62	
	BSTATE-GGA[38]	2.52		6.39	388	3.58	
	BSTATE-LDA[30]	2.556		6.32	376	3.5	
	SIESTA-GGA/PBE[39]	2.549		6.413	374	3.54	
	CASTEP-GGA/PBE[40]	2.547		6.384	401		
	CASTEP-GGA[41]	2.516		6.385			
	CASTEP-LDA[29]			6.313			
Imm2	Present	2.5048	3.7325	7.7245	335.4	3.32	7.482
	VASP-GGA/PBE[31]	2.503	3.736	7.731	376		
	VASP-GGA/PBE[36]						
I-4m2	Present	2.5176		11.3793	338.0	3.32	7.509
	VASP-GGA/PBE[31]	2.525		11.323	376	3.9	
	CASTEP-GGA[35]	2.491		11.232	385.6		
	VASP-GGA/PBE[36]				381		
	SIESTA-GGA/PBE[39]	5.946[b]		11.395	385	3.57	
	CASTEP-GGA/PBE[40]	2.512		11.304	380	3.6	
	CASTEP-GGA[41]	2.521		11.189	371		
	CASTEP-LDA[29]	2.49			400		
Pmma	Present	2.4999	2.5236	11.4777	339.3	3.31	7.519
	CASTEP-GGA[35]	2.472	2.495	11.346	388.4		
	VASP-GGA/PBE[36]				373		
	CASTEP-GGA/PBE[43]	2.50	2.52	11.38	376		
c-BC_5	Experimental[24]	3.635			335 ± 8	4.5 ± 0.6	
		2.570[a]		6.296[a]			

[a]The lattice constants of c-BC_5 derived from[24] corresponding to P3m1,[37] which is thought to be the best match of the experimental data. [b]The lattice constants for the cubic primitive cell of I-4m2 phase.

consideration since it is predicted to be the best match of the experimental c-BC_5, and the slow decline in V/V_0 ratio along with rising pressure (V/V_0 is greater than 90% up to 40 GPa)[33,36] allow us to fit the optimization results to the Murnaghan equation of state (EOS)[54] which gives good accuracy under this circumstance.[55] In this respect, the other considered phases also seem to have almost the same tendency. The calculated bulk modulus (B) for P3m1 is found to be approximately 0.65% higher than the experimental value, which is reported at 300 K and zero pressure.[24] Other references in Table II for B overestimate it by a much greater percentage, whereas the pressure derivative of the bulk modulus (B') is underestimated by a lower percentage than our work, except for one,[30] compared to the experiment. Even so, anyone can reach a general conclusion that temperature increase (up to 300 K) causes a decrease in B and an increase in B' at a constant pressure for BC_5. From the results given in this paper, the most ultra-incompressible phase is Pmma with a bulk modulus of ~339 GPa

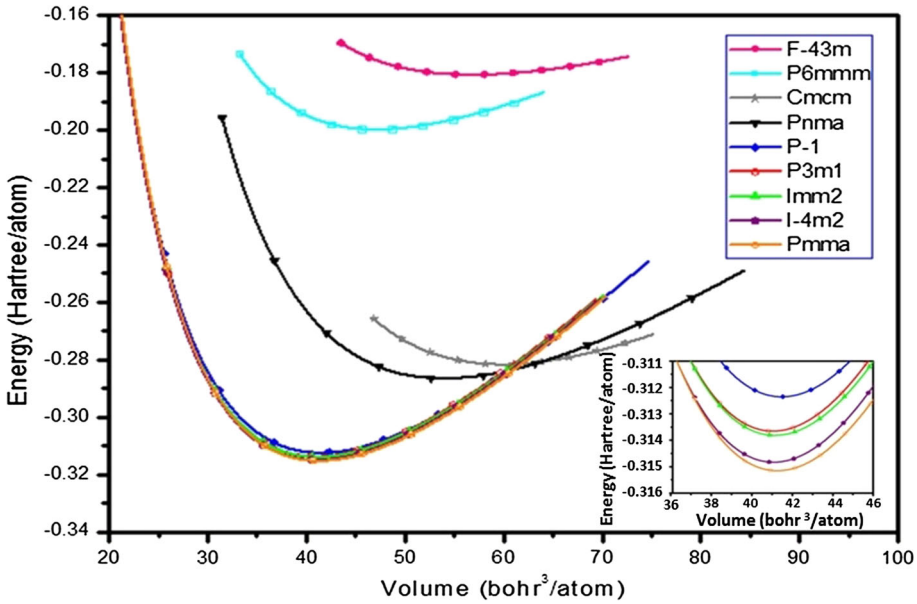

Fig. 2. The total energy versus volume graph for the nine phases of BC_5. The inset shows the zoomed-in image of the graph to distinguish easily the minimum energies of the five most stable phases from each other.

Table III. Calculated elastic constants (C_{ij}, GPa) of BC_5 phases

Phase	References	Stability	C_{11}	C_{12}	C_{13}	C_{14}	C_{22}	C_{23}	C_{33}	C_{44}	C_{55}	C_{66}
F-43m	Present	No	−62.3	153.3						−133.9		
P6/mmm	Present	No	156.9	263.7	183.9				359.8	−180.1		−53.4
Cmcm	Present	No	324.6	214.3	34.0		295.6	70.3	387.9	−0.3	−58.4	113.4
Pnma	Present	No	465.8	126.5	5.3		743.5	−10.2	6.9	13.0	−26.0	307.5
P3m1	Present	Yes	820.7	197.5	86.7	−107.5			1005.4	364.9		311.6
	M. Tool.-GGA/PBE[31]		862	166	88	−110			992	397		348
	BSTATE-GGA[32]		865	177	64	−101			1086	382		
	BSTATE-LDA[27]		931	194	69				1164	401		
	VASP-GGA/PBE[33]		832	181	90				1006	368		
	VASP-LDA[34]		872	205	113				1042	371		
	VASP-GGA/PBE[37]		821	194	87				1020	374		
	VASP-LDA[34]		882	212	100				1075	389		
	BSTATE-GGA[38]		865	177	64				1086	382		
	BSTATE-LDA[30]		931	194	69				1164	401		
	CASTEP-GGA[41]		792	220	85				1001	362		
	CASTEP-LDA[29]		868	216	92				1079	379		
Imm2	Present	Yes	860.9	199.0	28.5		763.1	178.3	944.6	436.7	273.6	448.1
I-4m2	Present	Yes	886.9	61.1	164.8				848.0	477.3		318.2
	M. Tool.-GGA/PBE[31]		775	175	169				830	479		304
	CASTEP-GGA[41]		852	92	169				841	482		307
	CASTEP-LDA[29]		913	86					906	513		313
Pmma	Present	Yes	984.2	45.5	121.4		876.4	144.7	894.5	455.3	432.4	346.1
	CASTEP-GGA[35]		988.7	17.7	163.0		960.5	171.5	842.8	490.0	493.6	338.4
	CASTEP-GGA/PBE[41]		791	178	153		785	178	791	472	445	472

(diamond: 442–446 GPa).[1–3] The order of incompressibility is Pmma > I-4m2 > P3m1 > Imm2 > P-1 for the five phases which possess the highest B values.

The total energy curves for nine phases of BC_5 as a function of the volume are displayed in Fig. 2, and Pmma is found to be the most energetically stable phase. The other four phases with the most minimum energies are in the order of I-4m2 < Imm2 < P3m1 < P-1, which should also be foreseen considering the cohesive energy values shown in Table II.

Table IV. Calculated shear modulus (G), Young modulus (E), Poisson ratio (ν), Vickers microhardness (H_v), G/B and B/G ratio (B values are calculated by using of elastic moduli), Debye temperature (Θ_D), and longitudinal, transverse and mean velocity (v_l, v_t and v_m) of BC_5 with the other theoretical studies

Phase	References	G (GPa)	E (GPa)	ν	H_v (GPa)	G/B	B/G	Θ_D (K)	v_l (m/s)	v_t (m/s)	v_m (m/s)
P-1	Present	422.7	917.9	0.0860	78.7	1.144	0.874	2035.9	16,937	11,400	12,447
	M. Tool.-GGA/PBE[31]	374			79						
P3m1	Present	389.0	868.8	0.1200	66.3	1.030	0.970	1957.4	16,575	10,918	11,954
	M. Tool.-GGA/PBE[31]	377	865	0.121	63[a]		0.95				
	BSTATE-GGA[32]	386	922	0.125	64		0.97				
	BSTATE-LDA[28]	410	803	0.15	84						
	VASP-GGA/PBE[33]	351	855	0.15	89						
	VASP-LDA[34]	372	884	0.11	60						
	VASP-GGA/PBE[36]	398	936	0.12	63						
	VASP-GGA/PBE[37]	419	865	0.121							
	VASP-LDA[34]	386	922	0.125							
	BSTATE-GGA[38]	410	788	0.149							
	BSTATE-LDA[30]	343	856	0.144							
	CASTEP-GGA[41]	374									
	CASTEP-LDA[29]										
Imm2	Present	391.9	873.2	0.1140	67.3	1.039	0.962	1964.7	16,617	10,968	12,005
	VASP-GGA/PBE[36]				65						
I-4m2	Present	397.3	882.5	0.1108	68.7	1.051	0.951	1977.1	16,680	11,035	12,076
	M. Tool.-GGA/PBE[31]	379	868	0.11	80						
	VASP-GGA/PBE[36]	391	921	0.116	71						
	CASTEP-GGA[41]	413									
	CASTEP-LDA[29]										
Pmma	Present	433.9	944.0	0.0878	79.3	1.136	0.879	2063.4	17,191	11,556	12,620
	VASP-GGA/PBE[36]	401			74						
	CASTEP-GGA/PBE[43]				71.5						

[a]The hardness is obtained using the valence electron density, bond length and ionicity via the equation given by Ref. 9 in Ref. 32.

Elastic Properties

The elastic constants play an important role in the determination of the mechanical properties and provide very important information about the nature of the interatomic forces. Particularly, they are also closely related to the stability, stiffness and strength of materials. The corresponding strains of stresses applied to a crystal within the elastic limit contain valuable data, building a bridge between the mechanical and dynamical behavior. Thus, carrying out such a calculation of elastic constants is essential to characterize the nature of materials under certain conditions generated by forces. In the present work, the elastic constants are calculated by utilizing the numerical first-principles method. Hence, the second-order elastic constants (C_{ij}) at 0 GPa and zero pressure for nine phases of BC_5 are obtained by the use of "stress–strain" relations and the results listed in Table III are consistent with the other theoretical studies.

The well-known Born–Huang elastic criteria are decisive in discussing the mechanical stability of a crystal system. The restrictive conditions in the cubic case are $C_{11} > 0$, $C_{12} > 0$, $C_{44} > 0$, $C_{12} > C_{44}$, $C_{11} + 2C_{12} > 0$ and $C_{11} - C_{12} > 0$; in the hexagonal case, they are $C_{11} > 0$, $C_{11} - C_{12} > 0$, $C_{44} > 0$ and $(C_{11} + C_{12})C_{33} - 2C_{12}^2 > 0$; in the orthorhombic case, they are $C_{ii} > 0$ (i = 1–6), $C_{11} + C_{12} - 2C_{12} > 0$, $C_{11} + C_{33} - 2C_{13} > 0$ and $C_{22} + C_{33} - 2C_{23} > 0$; and, lastly, in the tetragonal case, they are $C_{ii} > 0$ (i = 1, 3, 4, 6), $C_{11} - C_{12} > 0$, $C_{11} - 2C_{13} + C_{33} > 0$ and $2C_{11} + 2C_{12} + 4C_{13} + C_{33} > 0$; but also to forestall complexity, the necessary and sufficient criterion for a triclinic crystal symmetry with 21 independent elastic constants is that all eigenvalues of the stiffness coefficient matrix should be positive.[56] The matrix containing the elastic moduli in GPa for the triclinic P-1 phase of BC_5 is given as follows:

$$\begin{pmatrix} C_{11} & \cdots & C_{16} \\ \vdots & \ddots & \vdots \\ C_{61} & \cdots & C_{66} \end{pmatrix} = \begin{pmatrix} 889.5 & 118.6 & 103.0 & -11.5 & -22.4 & -115.0 \\ & 838.5 & 171.1 & 93.4 & -32.6 & 26.9 \\ & & 837.0 & -63.1 & 54.2 & 89.2 \\ & & & 331.7 & 30.5 & -26.3 \\ & & & & 411.5 & -46.8 \\ & & & & & 308.5 \end{pmatrix}, \quad (3)$$

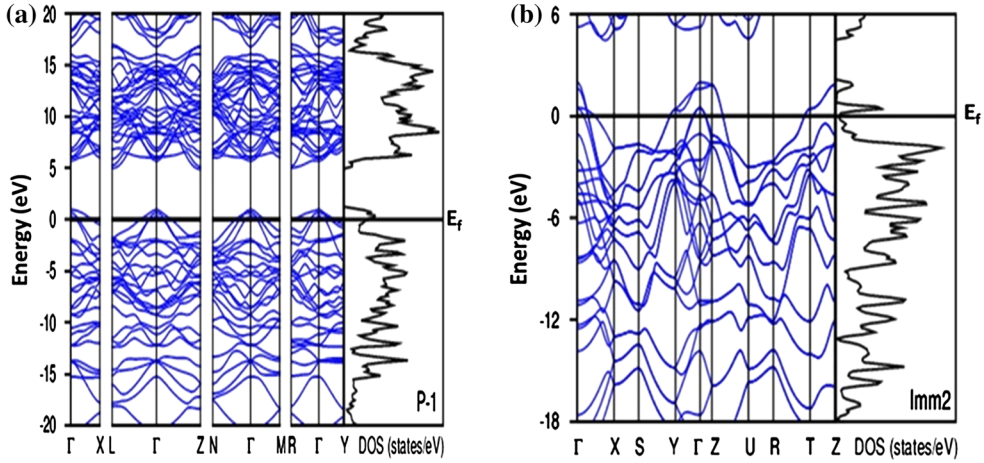

Fig. 3. The calculated band structures of BC_5 in P-1 (a) and Imm2 (b) phases, respectively.

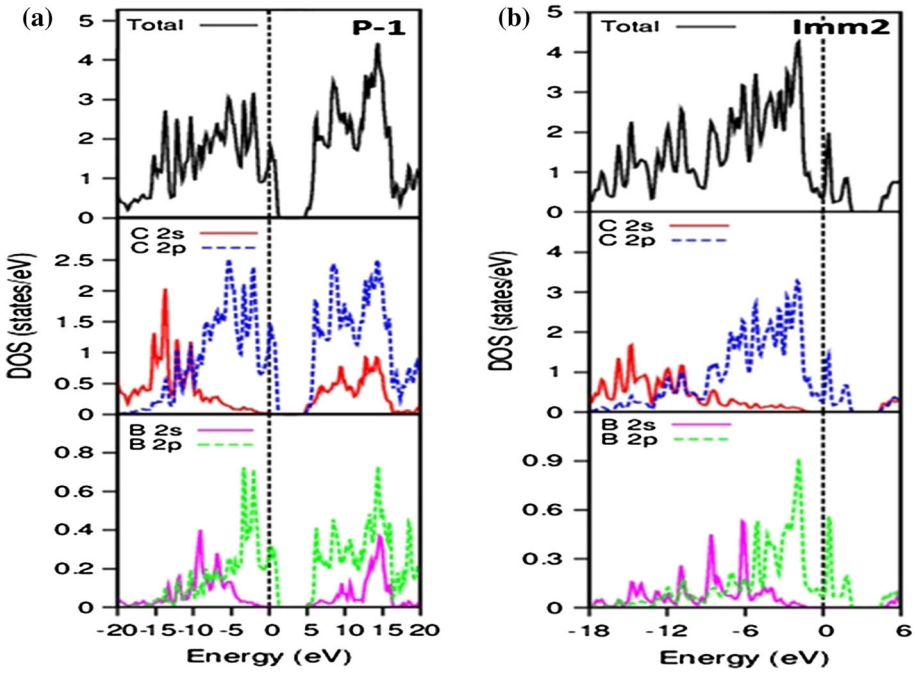

Fig. 4. The partial and total density of states (PDOS and TDOS) of BC_5 in P-1 (a) and Imm2 (b) phases, respectively.

and the related eigenvalues are found to be 244.1, 280.6, 441.7, 708.8, 824.2 and 1117.2. Under these circumstances, the examined phases are mechanically stable at ground state except F-43m, P6/mmm, Cmcm and Pnma, as can be seen in Table III.

As it is well-known, the mechanical characteristics of a material play a key role in determining the boundaries of its utilization in industrial applications, and so elastic properties are presented extensively in Table IV with the other theoretical references. Bulk and shear moduli for the phases with different crystal symmetries of BC_5 are obtained from Voigt–Reuss–Hill (VRH) approximation,[57–60] then Young modulus (E), Poisson ratio (ν), Debye temperature (Θ_D), longitudinal, transverse and mean velocity (v_l, v_t, v_m), respectively, are derived by the use of equations given below:

$$E=\frac{9GB}{(G+3B)};\quad \nu=\left(\frac{3B-2G}{6B+2G}\right);\quad \Theta_D=\frac{\hbar}{k}\left[\frac{3n}{4\pi}\left(\frac{N_A\rho}{M}\right)\right]^{\frac{1}{3}}v_m;$$
$$v_l=\left(\frac{3B+4G}{3\rho}\right)^{1/2};\quad v_t=\left(\frac{G}{\rho}\right)^{1/2};\quad v_m=\left[\frac{1}{3}\left(\frac{2}{v_t^3}+\frac{1}{v_l^3}\right)\right]^{\frac{1}{3}}, \tag{4}$$

where $\hbar$, k, N_A, n, M, and ρ are Planck and Boltzmann constants, Avogadro number, atom number per formula, molecule mass per formula,

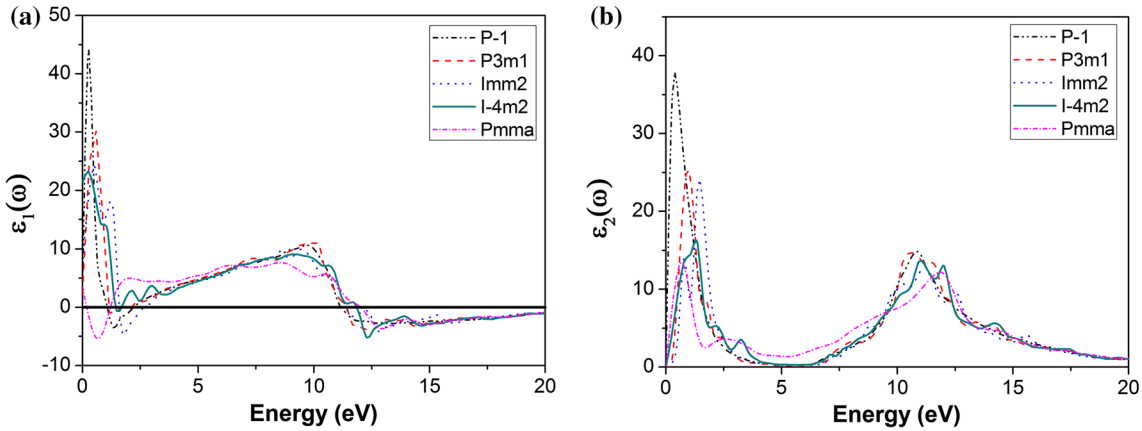

Fig. 5. The computed (a) real and (b) imaginary part of the dielectric function of BC_5 compound versus photon energy at 0 GPa and 0 K.

and density, respectively. Vickers microhardness (H) is calculated by the following relation:

$$H = C(G/B)^m G^n, \quad (5)$$

.where G/B is Pugh's modulus ratio[61] formed by the shear modulus (G, GPa) and bulk modulus (B, GPa). The values of m, n parameters and the proportional coefficient (C) assigned via a detailed data analysis are found to be 1.171, 0.591 and 1.887, respectively.[62]

It can be seen in Table IV that the estimations put forth about mechanical characteristics of the considered phases can be listed as follows: Pmma is the stiffest and the hardest one with the highest E of 944 GPa and H of 79.3 GPa among the others herein. It is remarkable that P3m1, Imm2 and I-4m2 can be predicted as superhard materials (with $H \geq 40$ GPa) while P-1 and Pmma are almost ultrahard (with $H \approx 80$ GPa).[63] The experimental value of H is found to be 71 GPa,[24] whereas 66.3 GPa is our computation for P3m1, which is thought to be the best match of the synthesized compounds. All of the phases have a Poisson ratio (v) of around 0.1, indicating that the covalent contributions to the atomic bonding are dominant (ionic for ~0.25); the interatomic forces are non-central (central for $0.25 < v < 0.5$)[61] and exhibit a brittle behavior due to the Pugh criterion, namely, having a B/G ratio of less than 1.75.[64,65] However, Zener anisotropy factors (A_1, $A_2$and A_3) point the measure of bonding anisotropy between atoms at different surfaces and equal to 1 for an isotropic material. A_1, A_2 and A_3 denote the elastic anisotropy values for {100}, {010}, {001} glide planes. The results for mechanically stable phases of BC_5 reveal they all show an anisotropic character deviating from 1 through the specified orientations, but only A_3 for P3m1, the value of which corresponds to 1, indicating an isotropic manner.

Electronic Properties

The electronic band structure, along with the various symmetry lines, and the density of states (DOS) are computed in order to understand the differences in the chemical bonding between them. In order to gain a better understanding of the electronic behavior and chemical bonding of BC_5, the electronic band structure along high-symmetry points in the Brillouin zone and total DOS (TDOS) under zero pressure and temperature are gathered for P-1 and Imm2 phases, which are not available in the literature, respectively, in Fig. 3a and b by means of using the equilibrium lattice constants. The Fermi level is indicated by a dotted horizontal line. The band structures of these phases are closely related to one another. It is shown that BC_5 exhibits a metallic feature due to the bands across the Fermi level as well as a non-zero DOS value at the Fermi level and, hence, there is no energy gap, which is in accordance with others' works.[31,36] It is well-known that most superhard materials with strong covalent bonds are semiconductors or insulators, and diamond shows insulator properties as indicated in the literature.[24,28,32] Unexpectedly, the BC_5 crystal for investigated phases exhibits a metallic character since the band gap around the Fermi level could not be observed.

To clarify the contribution of each orbital of B and C atoms, partial DOS (PDOS) for BC_5 are computed for P-1 and Imm2 phases, respectively as given in Fig. 4a and b. The total DOS curves for the two BC_5 bulk phases are similar to each other, especially in the low-energy region. These spectra have one common feature, which is the absence of a band gap in the neighborhood of the Fermi level, which indicates that all of them have metallic characteristics. The DOS graphs of the metallic BC_5 compounds for two phases show the PDOS with almost the same shape. In the DOSs of the given two phases, there is a pseudogap which can be defined as the borderline between the bonding and anti-bonding states. From the PDOSs, the carbons are found to have more contribution to the bonding states than the boron atoms, as given in the previous studies.[31,36] This is the display of a polar covalent bond for the coupling of B and C atoms. The lowest valence band between nearly −15 eV and

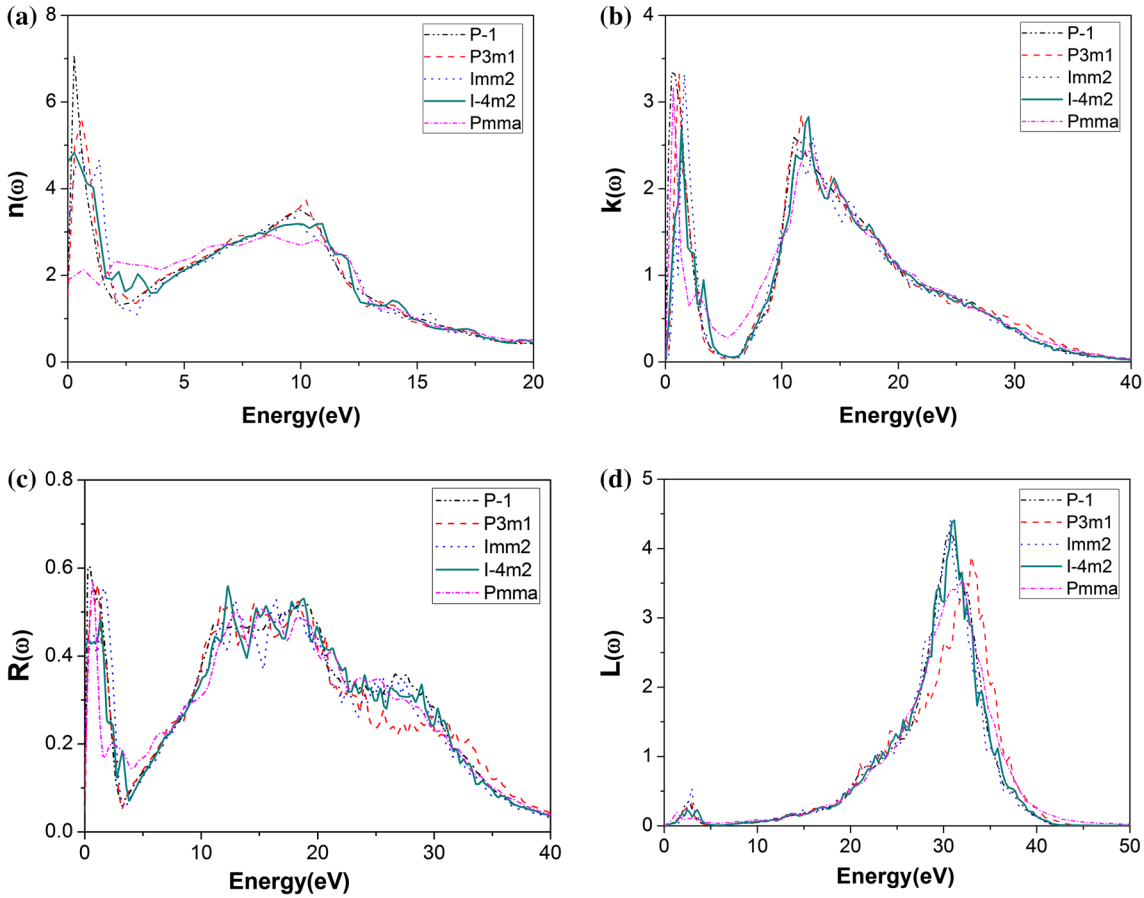

Fig. 6. The computed (a) refractive index $n(\omega)$, (b) extinction coefficient $k(\omega)$, (c) reflectivity $R(\omega)$ and (d) electron energy loss spectrum $L(\omega)$ of BC_5 compound versus photon energy at 0 GPa and 0 K.

−10 eV consists mainly of C-2*s* states with a minor contribution coming from B-2*s*. The DOS shape of B *p* and C *p* from −10 eV to 1 eV are very similar, indicating a strong hybridization between them. The large overlap between energy states from C atoms and that from B atoms indicates that strong hybrid bonds are formed between B and C atoms in BC_5. It is obvious that strong covalent bonds and a highly symmetrical structure are critical for the high hardness of diamond. The valence bands above the Fermi level originate mostly from the *p* and *s* orbitals of C atoms; small contributions from the *p* and *s* orbital of B atoms may also be observed.

Optical Properties

Now, we turn our attention to the optical properties of BC_5. The optical analysis reflect the band structure and other spectral information, and describe the macroscopic linear optical response of solids. As a function of photon energy, the calculated real and imaginary parts of the dielectric function $\varepsilon(\omega)$ are given in Fig. 5a and b up to 15 eV along the [101] direction for P-1, P3m1, Imm2, I-4m2 and Pmma phases of BC_5 which are mechanically stable. The static real parts of the dielectric function $\varepsilon_1(0)$ are found to be 2.93, 2.403, 8.115, 21.321 and 3.571 for P-1, P3m1, Imm2, I-4m2 and Pmma phases of BC_5, respectively. For frequencies larger than about 11.3 eV, 11.6 eV, 11.59 eV, 12.01 eV and 12.03 eV, the real part becomes negative for P-1, P3m1, Imm2, I-4m2 and Pmma phases of BC_5, respectively. As it can be seen in Fig. 5b, this compound has two major groups of the peaks. The first peaks of the imaginary part of the dielectric function $\varepsilon_2(\omega)$ are located at 0.38, 0.94, 1.453, 1.289 and 0.644 eV for P-1, P3m1, Imm2, I-4m2 and Pmma phases of BC_5, respectively, which are related to interband transitions between the valence and conduction bands. The calculated second peak values of the imaginary part of the dielectric function $\varepsilon_2(\omega)$ are 10.83 eV, 10.59 eV, 11.22 eV, 11.04 eV and 11.96 eV for P-1, P3m1, Imm2, I-4m2 and Pmma phases of BC_5, respectively.

The computed refractive index $n(\omega)$, extinction coefficient $k(\omega)$, reflectivity $R(\omega)$ and energy loss function $L(\omega)$ are estimated by Kramers–Kronig relations.[66,67] Our results are plotted in Fig. 6a, b, c, and d. The calculated refractive index is given in Fig. 6a for P-1, P3m1, Imm2, I-4m2 and Pmma phases of BC_5. While the predicted values of perpendicular static refractive index $n(0)$ are 1.71, 1.55,

2.84, 4.62 and 1.89, the main peak values of refractive index for P-1, P3m1, Imm2, I-4m2 and Pmma phases of BC_5 are 7.011 at 0.28 eV, 5.63 at 0.51 eV, 4.93 at 0.49 eV, 4.83 at 0.25 eV and 2.16 at 0.53 eV, respectively. In Fig. 6b, we have calculated the extinction coefficients for P-1, P3m1, Imm2, I-4m2 and Pmma phases of BC_5 to be 3.30, 3.33, 3.31, 2.67 and 3.15, respectively. As it can be seen in Fig. 6c, while the static reflectivity $R(0)$ values are 0.068, 0.046, 0.23, 0.41 and 0.094, the maximum values of that is about 0.63 at 0.33 eV, 0.55 at 1.14 eV, 0.55 at 1.61 eV, 0.47 at 1.38 eV and 0.56 at 0.67 eV for P-1, P3m1, Imm2, I-4m2 and Pmma phases of BC_5, respectively. Lastly, energy loss function, which is an important quantity describing the energy loss of a fast electron passing through a material, is given in Fig. 6d for these phases of the BC_5 compound. The maximum peaks in the energy loss function indicate that plasmon resonance occurs at around 30.65 eV, 33.03 eV, 30.77 eV, 31.02 eV, and 32.11 eV for P-1, P3m1, Imm2, I-4m2 and Pmma phases of BC_5, respectively. From these results, it can be concluded that the plasma frequency of P3m1 phase is the largest one.

Vibrational and Thermal Properties

Phonons are the elementary excitations that influence some physical properties, especially the thermodynamic behavior. Phonon frequencies from first-principles are calculated using well-tested DFT software,[66,67] which can calculate crystalline structures, electronic bands, elastic properties and so-called Hellmann–Feynman (HF) forces.

To calculate the phonon dispersion relation and phonon density of states for P-1, Imm2 and Pmma phases of the BC_5 compound, the density functional perturbation theory using the force constant method has been utilized. For this phonon computation, PHONOPY code[53] with a $2 \times 2 \times 2$ supercell is used. The phonon dispersion curves together with the total phonon density and partial phonon DOS are displayed in Fig. 7a, b, and c for P-1, Imm2 and Pmma phases of BC_5, and there are 12, 6 and 24 atoms in the unit cell, respectively. Thus, there should be 33, 15 and 69 optical modes and three acoustic modes for investigated phases, respectively. In Ref. 31, the phonon frequencies of the P-1 phase of BC_5 are found to be unstable at 0 K, while this phase is surprisingly dynamically stable in our study. However, Yao et al.[31] predicted that P-1 might be synthesized at high temperatures because of providing mechanical stability conditions. Much to our regret, there aren't any plotted phonon band structures for P-1 in the other studies to compare with our result.

It can be seen in Fig. 7a, b, and c that no imaginary phonon frequencies are found for calculated phases of BC_5, which indicates that it can be stable at 0 K. It is also important to notice that in the three investigated phases of BC_5, the highest calculated optical frequencies are obtained for Pmma phase while the smallest ones are obtained for P-1 phase for BC_5. There is no gap between the acoustic and optical modes for all of the three phases of BC_5 compound due to the close masses of B and C atoms. Also, it can be seen that there are nearly flat optical mode frequencies in the high-frequency region for all calculated stable phases of BC_5. The flat regions of the phonon dispersion curves, which stand for the peaks in the partial phonon DOS, indicate localization of the states, i.e. they act as atomic states.[68] The atoms have different contributions to the phonon DOS that can be based on the different mass of the constituted atoms. As can be also seen in Fig. 7a, b, and c, the phonon PDOS of

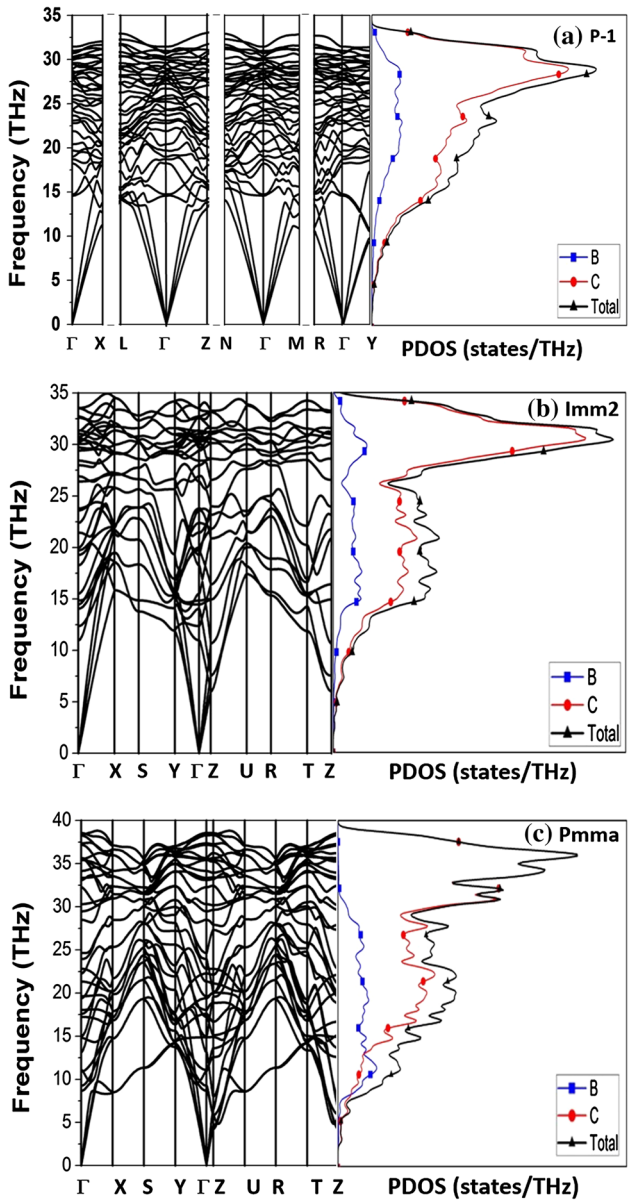

Fig. 7. The phonon frequencies and partial phonon density of state (PDOS) of BC_5 P-1 (a), Imm2 (b) and Pmma (c) phases, respectively.

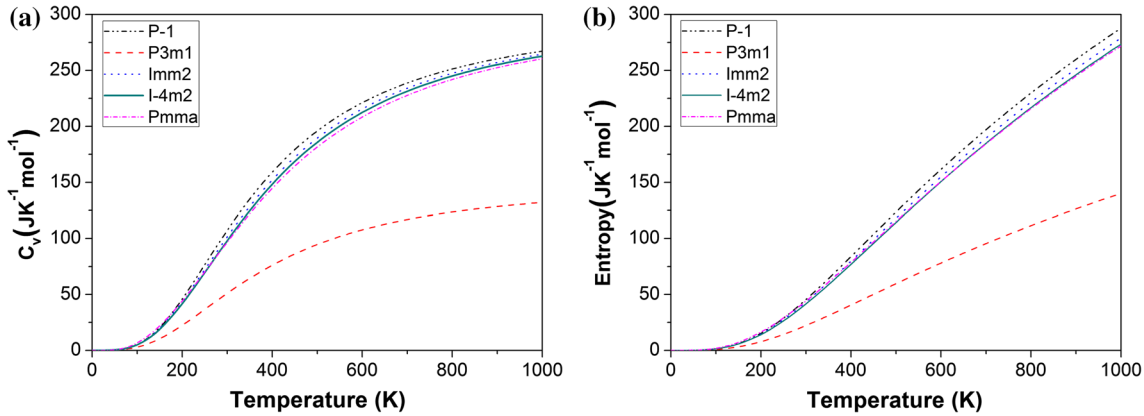

Fig. 8. The calculated heat capacity (a) and entropy (b) related to thermal properties for BC_5.

BC_5 has three regions: in the first region (acoustic mode), the main contribution stems from C; the main contribution of the middle region for BC_5 (lower optical mode) stems from C and a small amount of B; in the third region (upper optical mode), the vibrations of the C atom are predominant, while B has a very small contribution.

Phonon dispersion curves are important in analyzing dynamical behavior and thermal properties, such as constant volume heat capacity (C_v), Helmholtz free energy (F), entropy (S) and internal energy (E). Using the quasi-harmonic approximation, the temperature correlation of the C_v and S of BC_5 is given by the following equations[69]:

$$C_v = \sum_{qj} C_{qj} = \sum_{qj} k_B \left(\frac{\hbar\omega_{qj}}{k_B T}\right)^2 \frac{\exp\left(\frac{\hbar\omega_{qj}}{k_B T}\right)}{\left[\exp\left(\frac{\hbar\omega_{qj}}{k_B T}\right) - 1\right]^2}, \quad (6)$$

$$S = \frac{1}{2T}\sum_{qj} \hbar\omega_{qj} \coth\left[\frac{\hbar\omega_{qj}}{2k_B T}\right] - k_B \sum_{qj} In\left[2\sinh\left(\frac{\hbar\omega_{qj}}{2k_B T}\right)\right]. \quad (7)$$

In Fig. 8a, the calculated heat capacity at constant volume as a function of temperature for the five dynamically stable phases have been given. From this figure, the heat capacity increases linearly with the temperature ($\sim T <$ 300 K), but the rate of increase is mild especially at high pressures since the heat capacity reaches the classical Dulong–Petit limit. The obtained values of heat capacity at constant volume and 300 K are 107.18 J mol^{-1}/K, 51.02 J mol^{-1}/K, 101.33 J mol^{-1}/K, 97.97 J mol^{-1}/K and 96.65 J mol^{-1}/K for P-1, P3m1, Imm2, I-4m2 and Pmma phases of BC_5, respectively.

The changes of the entropy of all investigated phases of BC_5 from 0 K to 1000 K under 0 GPa pressure are shown in Fig. 8b. We can see in Fig. 8b that their entropy values are zero at 0 K, while at low temperature, the entropy rises with temperature and the change of entropy is small above about 300 K. The calculated values of entropy at 300 K are given as 45.45 J mol^{-1}/K, 22.22 J mol^{-1}/K, 43.27 J mol^{-1}/K, 41.53 J mol^{-1}/K and 44.10 J mol^{-1}/K for P-1, P3m1, Imm2, I-4m2 and Pmma phases of BC_5, respectively. Generally, the temperature alternation of thermodynamical functions shows a similar tendency for these phases of the BC_5 compound.

CONCLUSIONS

In summary, we have performed a comprehensive theoretical study on multiphase material BC_5, and it is predicted that Pmma is the most energetically stable. BC_5 may be experimentally obtained in different phases at high pressure and high temperature due to the metastable character, having the thermodynamically stable P–T region such as graphite and fullerene. Moreover, the five (P-1, P3m1, Imm2, I-4m2 and Pmma) phases are found to be mechanically and dynamically stable at the ground state. Remarkably, Vickers hardness calculations put forth that P3m1, Imm2 and I-4m2 can be classified as superhard materials (with $H \geq 40$ GPa) while P-1 and Pmma are almost ultrahard (with $H \approx 80$ GPa). Although most of the superhard materials exhibit insulating or semiconducting behavior, analysis of the electronic band structure indicates metallicity for these considered phases. We expect to contribute further to the research on designing novel boride materials with excellent mechanical performance.

REFERENCES

1. H.J. McSkimin and P. Andreatch, *J. Appl. Phys.* 43, 2944 (1972).
2. R. Vogelgesang, A.K. Ramdas, S. Rodriguez, M. Grimsditch, and T.R. Anthony, *Phys. Rev. B* 54, 3989 (1996).
3. F. Occelli, P. Loubeyre, and R. LeToullec, *Nat. Mater.* 2, 151 (2003).
4. M.H. Nazaré and A.J. Neves, *Properties, Growth and Applications of Diamond*, 1st ed. (London: INSPEC, IEE, 2001), pp. 349–431.
5. A. Upadhyay, A.K. Singh, and A. Kumar, *Comput. Mater. Sci.* 89, 257 (2014).

6. H.-J. Cui, X.-L. Sheng, Q.-B. Yan, Z.-G. Zhu, Q.-R. Zheng, and G. Su, *Comput. Mater. Sci.* 98, 129 (2015).
7. E.A. Ekimov, V.A. Sidorov, E.D. Bauer, N.N. Melnik, N.J. Curro, J.D. Thompson, and S.M. Stishov, *Nature* 428, 542 (2004).
8. J.E. Moussa and M.L. Cohen, *Phys. Rev. B* 77, 064518 (2008).
9. H.-Y. Chung, M.B. Weinberger, J.B. Levine, A. Kavner, J.-M. Yang, S.H. Tolbert, and R.B. Kaner, *Science* 316, 436 (2007).
10. D.M. Teter and R.J. Hemley, *Science* 271, 53 (1996).
11. V.L. Solozhenko, N.A. Dubrovinskaia, and L.S. Dubrovinsky, *Appl. Phys. Lett.* 85, 1508 (2004).
12. P.V. Zinin, L.C. Ming, I. Kudryashov, N. Konishi, M.H. Manghnani, and S.K. Sharma, *J. Appl. Phys.* 100, 013516 (2006).
13. J.E. Lowther, *J. Phys. Condens. Matter* 17, 3221 (2005).
14. S. Chen and X.G. Gong, *Phys. Rev. Lett.* 98, 015502 (2007).
15. V.L. Solozhenko, D. Andrault, G. Fiquet, M. Mezouar, and D.C. Rubie, *Appl. Phys. Lett.* 78, 1385 (2001).
16. Y. Zhao, D.W. He, L.L. Daemen, T.D. Shen, R.B. Schwarz, Y. Zhu, D.L. Bish, J. Huang, J. Zhang, G. Shen, J. Qian, and T.W. Zerda, *J. Mater. Res.* 17, 3139 (2002).
17. N.V. Novikov, *J. Mater. Proc. Technol.* 161, 169 (2005).
18. S. Vepřek, *J. Vac. Sci. Technol. A* 17, 2401 (1999).
19. E. Knittle, R.B. Kaner, R. Jeanloz, and M.L. Cohen, *Phys. Rev. B* 51, 12149 (1995).
20. K. Sakaushi and M. Antonietti, *Bull. Chem. Soc. Jpn.* 88, 386 (2015).
21. R. Kumar and A. Parashar, *Nanoscale* 8, 22 (2016).
22. H. Zhang, C.J. Tong, Y. Zhang, Y.N. Zhang, and L.M. Liu, *J. Mater. Chem. A* 3, 9632 (2015).
23. S.Y. Yuan, J.L. Bao, L.N. Wang, Y.Y. Xia, D.G. Truhlar, and Y.G. Wang, *Adv. Energy Mater.* 6, 1501733 (2016).
24. V.L. Solozhenko, O.O. Kurakevych, D. Andrault, Y.L. Godec, and M. Mezouar, *Phys. Rev. Lett.* 102, 015506 (2009).
25. Q. Hu, Q. Wu, Y. Ma, L. Zhang, Z. Liu, J. He, H. Sun, H.-T. Wang, and Y. Tian, *Phys. Rev. B* 73, 214116 (2006).
26. R.F. Zhang, S. Veprek, and A.S. Argon, *Phys. Rev. B* 80, 233401 (2009).
27. N. Nakae, J. Ishisada, H. Dekura, and K. Shirai, *J. Phys. Conf. Ser.* 215, 012116 (2010).
28. Y.-J. Wang and C.-Y. Wang, *J. Appl. Phys.* 106, 043513 (2009).
29. M. Calandra and F. Mauri, *Phys. Rev. Lett.* 101, 016401 (2008).
30. P. Lazar and R. Podloucky, *Appl. Phys. Lett.* 94, 251904 (2009).
31. Y. Yao, J.S. Tse, and D.D. Klug, *Phys. Rev. B* 80, 094106 (2009).
32. Y.C. Liang, W.Q. Zhang, J.Z. Zhao, and L.F. Chen, *Phys. Rev. B* 80, 113401 (2009).
33. C. Jiang, Z. Lin, and Y. Zhao, *Phys. Rev. B* 80, 184101 (2009).
34. S.M. Nkambule and J.E. Lowther, *Solid State Commun.* 150, 133 (2010).
35. S. Xi, *Chin. Phys. Lett.* 27, 016101 (2010).
36. Q. Li, H. Wang, Y. Tian, Y. Xia, T. Cui, J. He, Y. Ma, and G. Zou, *J. Appl. Phys.* 108, 023507 (2010).
37. W.J. Zhao and Y.X. Wang, *Solid State Commun.* 151, 478 (2011).
38. Q. Zhang, S.M. Wang, and Y.C. Liang, *J. Zhejiang Univ. Sci. A (Appl. Phys. Eng.)* 12, 177 (2011).
39. J.-D. Zhang and X.-L. Cheng, *Comput. Mater. Sci.* 50, 2249 (2011).
40. J.-D. Zhang, X.-L. Cheng, and D.-H. Li, *Phys. B* 406, 2574 (2011).
41. D.-H. Li, W.-J. Su, and X.-L. Zhu, *Acta Phys. Sin.* 61, 023103 (2012).
42. A.S. Mikhaylushkin, X. Zhang, and A. Zunger, *Phys. Rev. B* 87, 094103 (2013).
43. M.M. Li, X. Fan, and W.T. Zheng, *J. Phys. Condens. Matter* 25, 425502 (2013).
44. P. Hohenberg and W. Kohn, *Phys. Rev.* 136, B864 (1964).
45. W. Kohn and L.J. Sham, *Phys. Rev.* 140, A1133 (1965).
46. P.E. Blöchl, *Phys. Rev. B* 50, 17953 (1994).
47. J.P. Perdew, K. Burke, and M. Ernzerhof, *Phys. Rev. Lett.* 77, 3865 (1996).
48. G. Kresse and J. Furthmuller, *Phys. Rev. B* 54, 11169 (1996).
49. H.J. Monkhorst and J.D. Pack, *Phys. Rev. B* 13, 5188 (1976).
50. Y.L. Page and P. Saxe, *Phys. Rev. B* 65, 104104 (2002).
51. M.J. Mehl, J.E. Osburn, D.A. Papaconstantopoulos, and B.M. Klein, *Phys. Rev. B* 41, 10311 (1990).
52. S.Q. Wang and H.Q. Ye, *Phys. Status Solidi (b)* 240, 45 (2003).
53. F.P. Bundy, W.A. Bassett, M.S. Weathers, R.J. Hemley, H.K. Mao, and A.F. Goncharov, *Carbon* 34, 141 (1996).
54. F.D. Murnaghan, *Proc. Natl. Acad. Sci. USA* 30, 244 (1944).
55. R.J. Angel, *High-Pressure Crystallography*, ed. A. Katrusiak and P. McMillan (Dordrecht: Springer, 2004), p. 21.
56. F. Mouhat and F.-X. Coudert, *Phys. Rev. B* 90, 224104 (2014).
57. W. Voigt, *Lehrbuch der Kristallphysik*, 1st ed. (Leipzig: Teubner, 1928).
58. W. Voigt, *Wied. Ann.* 38, 573 (1889).
59. A. Reuss and Z. Angew, *Math. Mech.* 9, 49 (1929).
60. R. Hill, *Proc. Phys. Soc. Lond.* 65, 349 (1952).
61. S.F. Pugh, *Philos. Mag. (Ser. 7)* 45, 823 (1954).
62. X.-Q. Chen, H. Niu, D.Z. Li, and Y.Y. Li, *Intermetallics* 19, 1275 (2011).
63. V. Kanyanta, *Microstructure-Property Correlations for Hard, Superhard, and Ultrahard Materials*, ed. V. Kanyanta (Cham: Springfield, 2016), p. 4.
64. D.G. Pettifor, *Mater. Sci. Technol.* 8, 345 (1992).
65. R.A. Johnson, *Phys. Rev. B* 37, 3924 (1988).
66. S. Adachi, *Properties of Group-IV, III-V and II-VI Semiconductors*, 1st ed. (Chichester: Wiley, 2005), pp. 213–214.
67. P. Ravindran, A. Delin, B. Johansson, O. Eriksson, and J.M. Wills, *Phys. Rev. B* 59, 1776 (1999).
68. A. Togo, L. Chaput, I. Tanaka, and G. Hug, *Phys. Rev. B* 81, 174301 (2010).
69. A. Togo and I. Tanaka, *Scr. Mater.* 108, 1 (2015).